Supporting Information

1 Molecular Dynamics Simulations

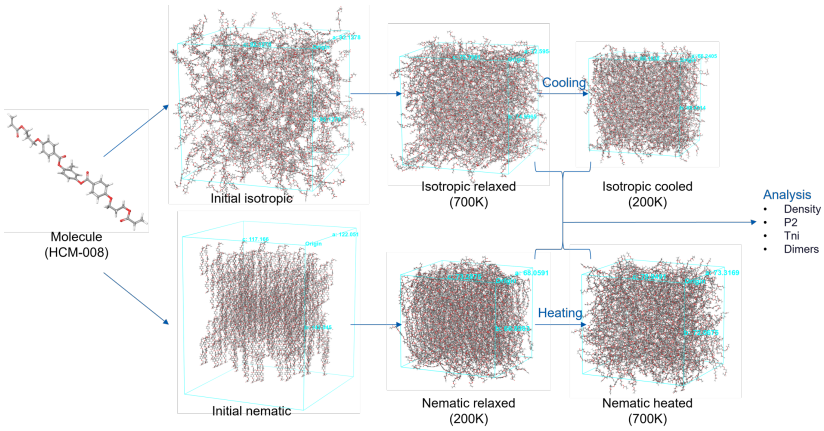

Figure S1: Molecular dynamics cooling and heating protocol for the nematic phase transition computations.

All computational systems for molecular dynamics (MD) were built and simulated using Schrödinger's Materials Science Suite Release 2024-3, employing the OPLS4 force field.[1–3] Initially, molecules of a liquid crystal candidate were packed into a simulation cell using the disordered system builder to create a disordered cell, with approximately 30,000 atoms and a density of 0.5 g/cm^3. To ensure statistical reliability, two sets of randomly packed simulation cells were generated for each candidate, with simulations run on both sets.

For equilibration, MD simulations were performed at 700 K. The procedure included 20 ps of Brownian dynamics in NVT ensemble (number of atoms [N], volume [V], and temperature [T] are held constant) at 10 K, followed by 20 ps of Brownian dynamics in NPT ensemble (number of atoms, pressure [P], and temperature are held constant) at 1 atm and 100 K, then 100 ps MD simulation in NPT ensemble at 1 atm and 300 K, and finally 10 ns MD simulation in NPT ensemble at 1 atm and 700 K. It was ensured that the potential energy and density of systems had reached a consistent average value at the end of the equilibration procedure. We used the Nosé–Hoover thermostat and the Martyna–Tobias–Klein barostat during this process.[4–6]

After equilibration at 700 K, the systems were gradually cooled to 200 K to observe any transition to an ordered state. Cooling was simulated in the NPT ensemble at 1 atm, with temperature decrements of 2 K and 2 ns of simulation per step, totaling 500 ns and achieving a cooling rate of 1 K/ns. At the end of each temperature step, the order parameter (P2) was calculated from the structure with molecular directions defined by the principal axes of iner-

tia. The transition temperature (T_{ni}) was identified as the lowest temperature where P2 crossed the threshold value of 0.2. T_{ni} values from the two replicates were averaged. To further confirm the presence of the liquid crystal phase, for selected molecules, a reverse simulation was performed, where the system was gradually heated from an ordered to a disordered state to check the observed phase transition temperatures from the cooling process.

2 Experimental UV-Vis Measurements

The polarization-dependent UV-Vis transmission and reflection spectra were recorded using a Cary 7000 spectrophotometer. Measurements were conducted over a wavelength range of 250 nm to 750 nm, with data collected in 1 nm increments and an averaging time of 0.5 sec per measurement. The spectral bandwidth of the incident light was set to 4 nm on the monochromator, further refined by a pair of 3-degree vertical slits and a 1-degree horizontal slit, producing a square beam approximately 4 mm in lateral length. Baseline measurements for 100% transmission and zero were obtained at a detector angle of 180 degrees, using air as the reference. Samples were mounted vertically and aligned with the detector at an incidence angle of 6 degrees using white light. Subsequent data collection was also conducted at a 6-degree angle of incidence, with the auto-polarizer set to 0 and 90 degrees for S and P polarized light, respectively.

3 Fitness Function Design

Fitness function 1 consists of three components: the transparency score ($S_{\text{transparency}}$), the average refractive index score ($S_{n_{\text{avg}}}$), and the anisotropic refractive index difference score ($S_{n_{\text{diff}}}$). The selection prioritizes molecules with high refractive indices while maintaining optical transparency. A molecule qualifies for scoring and ranking if it meets the following criteria:

1. The maximum absorption wavelength ($\lambda_{\max}$) is below 460 nm:

$$\lambda_{\max} < 460\,\text{nm}$$

2. The ratio of absorbance at $\lambda_{\max}$ to absorbance at 460 nm is greater than 1:

$$\frac{A(\lambda_{\max})}{A(460\,\text{nm})} \geq 1$$

3. The anisotropic refractive index difference, defined as Δn, is above 0.3:

$$\Delta n = n_e - n_o \geq 0.3$$

The transparency score is defined as a piecewise function:

$$S_{\text{transparency}} = \begin{cases} \log\left(\frac{A(460\,\text{nm})}{A(\lambda_{\max})}\right), & \text{if } \frac{A(\lambda_{\max})}{A(460\,\text{nm})} < 100 \\ 8, & \text{if } 100 \leq \frac{A(\lambda_{\max})}{A(460\,\text{nm})} < 1000 \\ 10, & \text{if } \frac{A(\lambda_{\max})}{A(460\,\text{nm})} \geq 1000 \end{cases}$$

The average refractive index score is defined as:

$$S_{n_{\text{avg}}} = n_{\text{avg}} \times 10$$

The anisotropic refractive index difference score ($S_{n_{\text{diff}}}$) is defined as:

$$S_{n_{\text{diff}}} = \Delta n \times 20 = (n_e - n_o) \times 20$$

Finally, the overall Fitness Function 1 score (S_{fitness1}) is computed as the sum of the three individual scores:

$$S_{\text{fitness1}} = S_{\text{transparency}} + S_{n_{\text{diff}}} + S_{n_{\text{avg}}}$$

Fitness function 2 consists of four components: the transparency score ($S_{\text{transparency}}$), the average refractive index score ($S_{n_{\text{avg}}}$), the anisotropic refractive index difference score ($S_{n_{\text{diff}}}$), and the maximum wavelength score ($S_{\lambda_{\max}}$). This function prioritizes molecules with high transparency while maintaining a high refractive index. A molecule qualifies for scoring and ranking if it meets the following criteria:

1. The average refractive index is above 1.5:

$$n_{\text{avg}} \geq 1.5$$

2. The anisotropic refractive index difference, defined as Δn, is above 0.3:

$$\Delta n = n_e - n_o \geq 0.3$$

The maximum wavelength score is defined as:

$$S_{\lambda_{\max}} = \frac{460 - \lambda_{\max}}{5}$$

The transparency score is defined as a piecewise function:

$$S_{\text{transparency}} = \begin{cases} \log\left(\frac{A(\lambda 460\text{nm})}{A(\lambda\text{max})}\right) \times 10 + S_{\lambda_{\max}}, & \text{if } \frac{A(\lambda\text{max})}{A(\lambda 460\text{nm})} \leq 10 \\ 30 + S_{\lambda_{\max}}, & \text{if } 10 \leq \frac{A(\lambda\text{max})}{A(\lambda 460\text{nm})} \leq 100 \\ 80 + S_{\lambda_{\max}}, & \text{if } 100 \leq \frac{A(\lambda\text{max})}{A(\lambda 460\text{nm})} \leq 1000 \\ 100 + S_{\lambda_{\max}}, & \text{if } \frac{A(\lambda\text{max})}{A(\lambda 460\text{nm})} \geq 1000 \end{cases}$$

The anisotropic refractive index difference score is defined as:

$$S_{n_{\text{diff}}} = \Delta n \times 20$$

The average refractive index score is defined as:

$$S_{n_{\text{avg}}} = n_{\text{avg}} \times 100$$

Finally, the overall Fitness Function 2 score (S_{fitness2}) is computed as the sum of the four individual scores:

$$S_{\text{fitness2}} = S_{\text{transparency}} + S_{n_{\text{diff}}} + S_{n_{\text{avg}}} + S_{\lambda_{\max}}$$

4 Tables

Table S1: The nematic transition temperature (T_{ni}) of the five commercial reactive mesogens: HCM-008, HCM-009, HCM-020, HCM-021, and HCM-083.

Sample	$T_{ni,\ avg}$ (K)	$T_{ni,\ cool_1}$ (K)	$T_{ni,\ cool_2}$ (K)	$T_{ni,\ heat_1}$ (K)	$T_{ni,\ heat_2}$ (K)
HCM-008	515	495	469	553	543
HCM-009	467	479	383	503	503
HCM-020	410	low	357	433	439
HCM-021	410	low	low	411	409
HCM-083	499	493	507	495	501

Table S2: The maximum absorption wavelengths (in nm) of the average spectra for the five reactive mesogens calculated via dimer pipeline (Dimer-xTB) and MD simulations (Dimer-MD), compared with experimental spectra (Experiment). The MD spectra were averaged from 200 dimers in the nematic phase, while the dimer pipeline spectra were averaged from the 8 lowest energy dimers. When compared to experiments, the mean absolute deviation (MAE) of the dimer-xTB approach is 9.4 nm and that of the Dimer-MD approach is 6.3 nm.

Approach	HCM-008	HCM-009	HCM-020	HCM-021	HCM-083
Dimer-xTB	274	273	268	254	259
Dimer-MD	260	262	254	250	252
Experiment	257	257	267	260	252

Table S3: Density, polarizability (α_{avg}), and isotropic refractive index (n_{avg}) values of the dimers and their constituent monomers (m_1, m_2) for four reactive mesogens and their various conformations.

Sample	Density (g/cm^3)					α_{avg}					n_{avg}				
	m_1	m_2	m_1+m_2	dimer	Δ%	m_1	m_2	m_1+m_2	dimer	Δ%	m_1	m_2	m_1+m_2	dimer	Δ%
HCM020-1	1.1732	1.1735	1.1733	1.1747	0.12	283.19	282.87	566.06	570.75	0.82	1.5439	1.5433	1.5436	1.5499	0.40
HCM020-2	1.1726	1.1733	1.1729	1.1739	0.08	283.50	283.21	566.71	572.33	0.98	1.5443	1.5440	1.5442	1.5513	0.46
HCM020-3	1.1728	1.1735	1.1732	1.1728	0.03	283.28	282.93	566.21	564.38	0.32	1.5435	1.5439	1.5437	1.5414	0.15
HCM020-4	1.1728	1.1728	1.1728	1.1728	0.00	283.18	283.29	566.46	563.78	0.48	1.5440	1.5437	1.5438	1.5407	0.20
HCM021-1	1.1540	1.1582	1.1561	1.1720	1.36	282.31	281.66	563.97	561.06	0.52	1.5233	1.5241	1.5237	1.5291	0.35
HCM021-2	1.1553	1.1560	1.1557	1.1596	0.33	283.81	284.13	567.94	565.55	0.42	1.5273	1.5284	1.5279	1.5274	0.04
HCM021-3	1.1573	1.1567	1.1570	1.1604	0.29	281.61	282.21	563.81	571.26	1.30	1.5235	1.5245	1.5240	1.5342	0.66
HCM021-4	1.1578	1.1578	1.1578	1.1580	0.02	281.58	282.00	563.58	569.08	0.97	1.5237	1.5247	1.5242	1.5304	0.41
HCM021-5	1.1571	1.1573	1.1572	1.1573	0.01	281.60	282.13	563.74	561.90	0.33	1.5234	1.5247	1.5241	1.5221	0.13
HCM083-1	1.1592	1.1592	1.1592	1.1589	0.02	282.06	282.05	564.11	563.04	0.19	1.5256	1.5255	1.5256	1.5242	0.09
HCM083-2	1.1591	1.1592	1.1592	1.1590	0.01	282.05	282.05	564.11	564.42	0.06	1.5255	1.5255	1.5255	1.5258	0.02
HCM083-3	1.1592	1.1592	1.1592	1.1588	0.03	282.05	564.10	564.10	561.46	0.47	1.5255	1.5255	1.5255	1.5224	0.20
HCM083-4	1.1591	1.1592	1.1592	1.1588	0.03	282.06	564.10	564.12	564.03	0.02	1.5255	1.5256	1.5256	1.5253	0.02
HCM083-5	1.1592	1.1592	1.1592	1.1590	0.02	282.05	564.12	564.10	562.13	0.35	1.5255	1.5255	1.5255	1.5233	0.15
HCM009-1	1.1620	1.1567	1.1593	1.1545	0.42	489.63	491.01	980.63	979.96	0.07	1.5449	1.5437	1.5443	1.5411	0.21

Table S4: The nematic transition temperature (T_{ni}) of ten candidate liquid crystal structures. Average and individual results are reported from MD cooling process for different random initializations of the systems.

Sample	$T_{ni,\ avg}$ (K)	$T_{ni,\ cool_1}$ (K)	$T_{ni,\ cool_2}$ (K)
Candidate1	<200	<200	<200
Candidate2	504	505	503
Candidate3	623	619	617
Candidate4	642	645	639
Candidate5	666	675	657
Candidate6	671	675	667
Candidate7	699	699	>700
Candidate8	>700	>700	>700
Candidate9	>700	>700	>700
Candidate10	>700	>700	>700

5 Figures

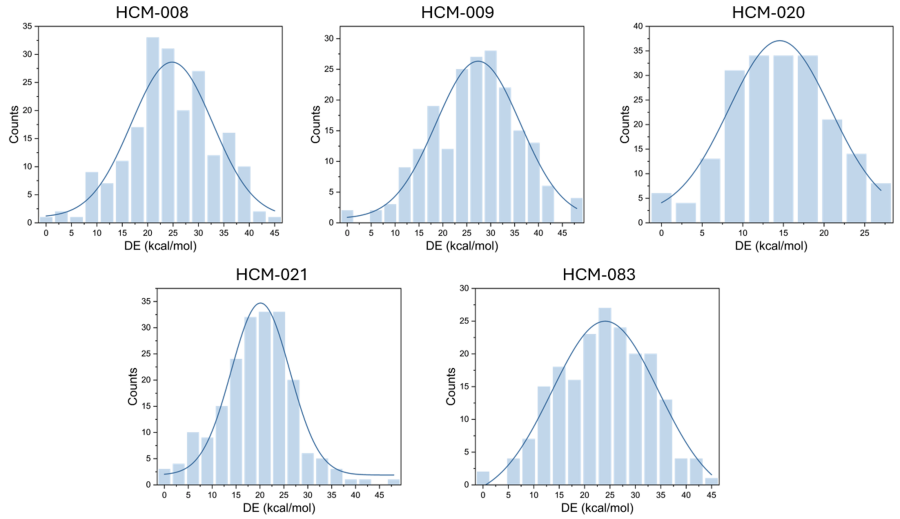

Figure S2: Energy distributions of 200 MD-extracted dimers from five commercial reactive mesogens in the nematic phase calculated using the GFN2-xTB method.

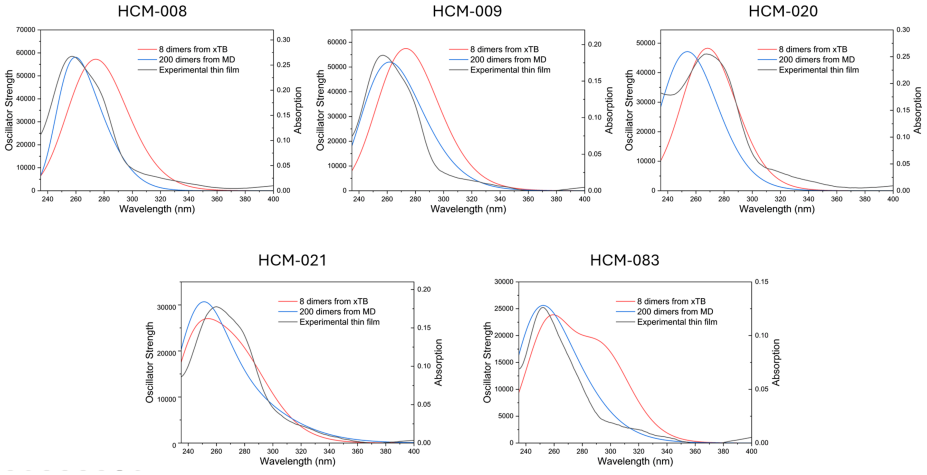

Figure S3: Experimental thin film absorption spectra of the five reactive mesogens. Each plot also contains average spectra of 200 MD-extracted dimers in nematic phase and average spectra for 8 dimers extracted from dimer generation pipeline.

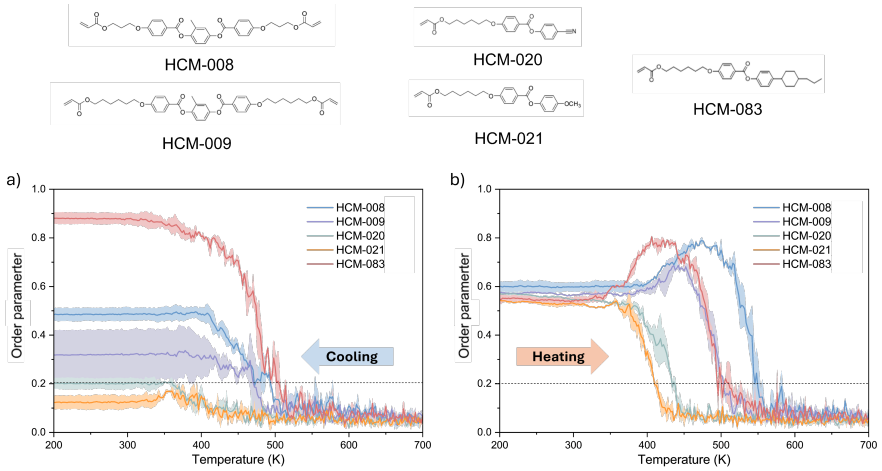

Figure S4: Order parameter as a function of temperature for HCM-008, HCM-009, HCM-020, HCM-021, and HCM-083 during the MD cooling and heating processes.

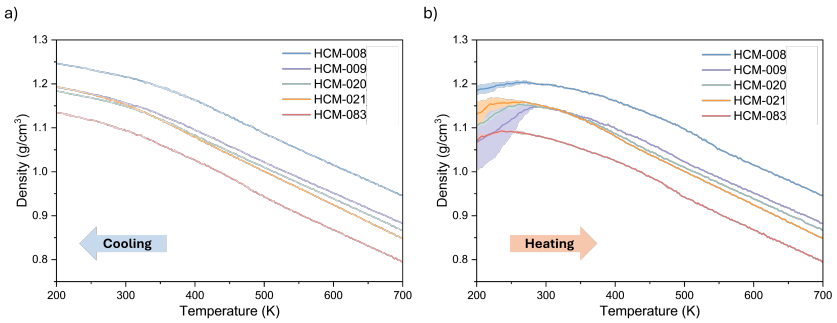

Figure S5: Density as a function of temperature for HCM-008, HCM-009, HCM-020, HCM-021, and HCM-083 during the MD cooling and heating processes.

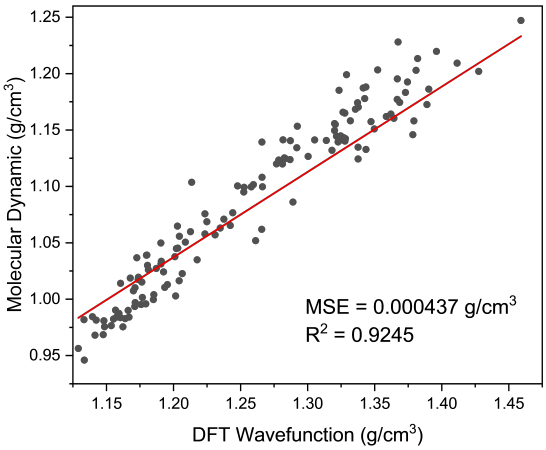

Figure S6: The density calculated by the van der Waals molecular volume via DFT wavefunctions compared to the cell density of the molecules at 298 K during MD cooling process from 700 K to 200 K.

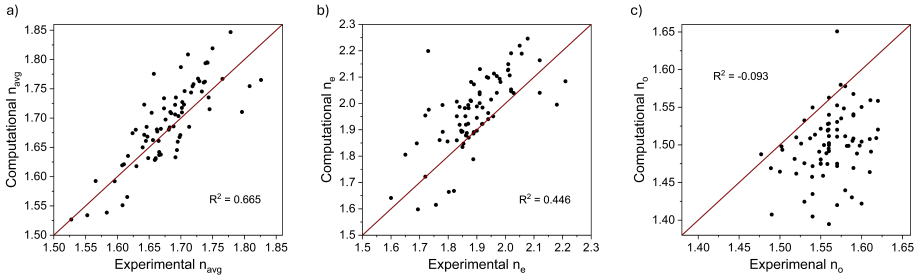

Figure S7: (a) n_{avg}, (b) n_e, and c) n_o refractive index comparisons of the 77 literature-reported liquid crystal small molecules obtained from DFT calculations using the M06-HF functional along with the ZPOL basis set and molecular volume calculated density approach.

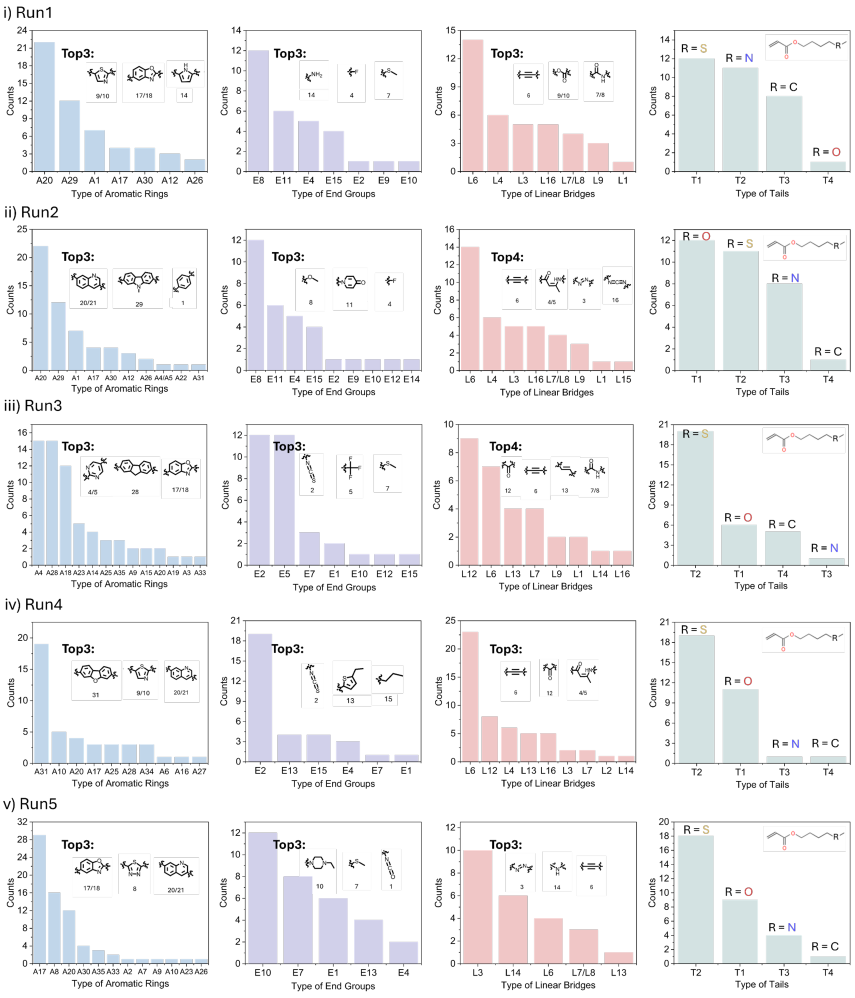

Figure S8: Frequency of the building blocks for Fitness function 1 and the top candidates for each component in monomer structure generation.

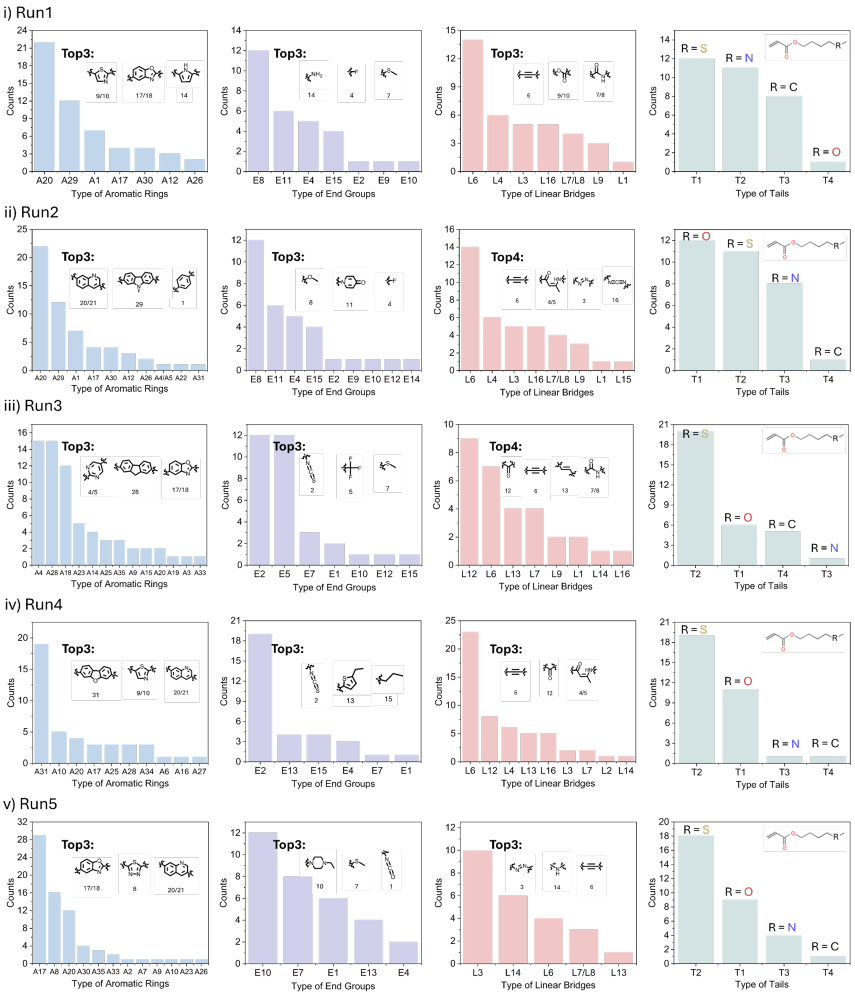

Figure S9: Frequency of the building blocks for Fitness function 2 and the top candidates for each component in monomer structure generation.

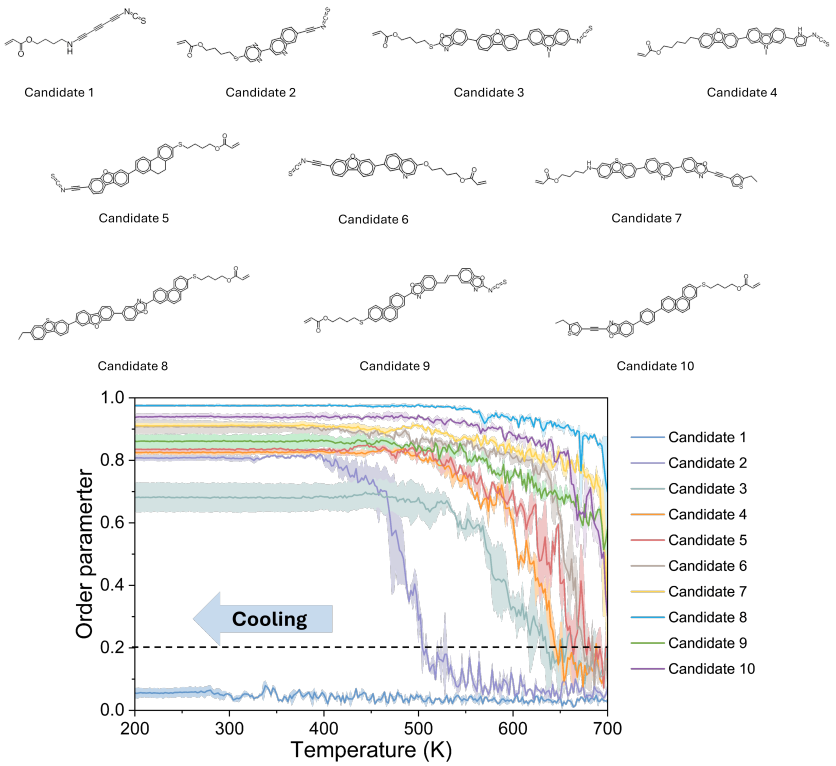

Figure S10: Order parameter as a function of temperature for all ten candidates during MD cooling process. For each candidate, the figure shows the average of the order parameter (darker colors), as well as the maximum and minimum values at the given temperature (lighter colors) for two MD cooling runs for different random initializations of the starting system. Overall, both runs are consistent for all candidates.

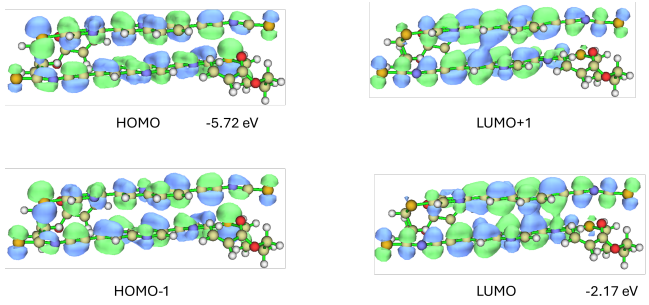

Figure S11: Molecular orbitals of Candidate 2, with the green and blue isosurfaces representing positive and negative values, respectively.

5.1 Building Blocks List

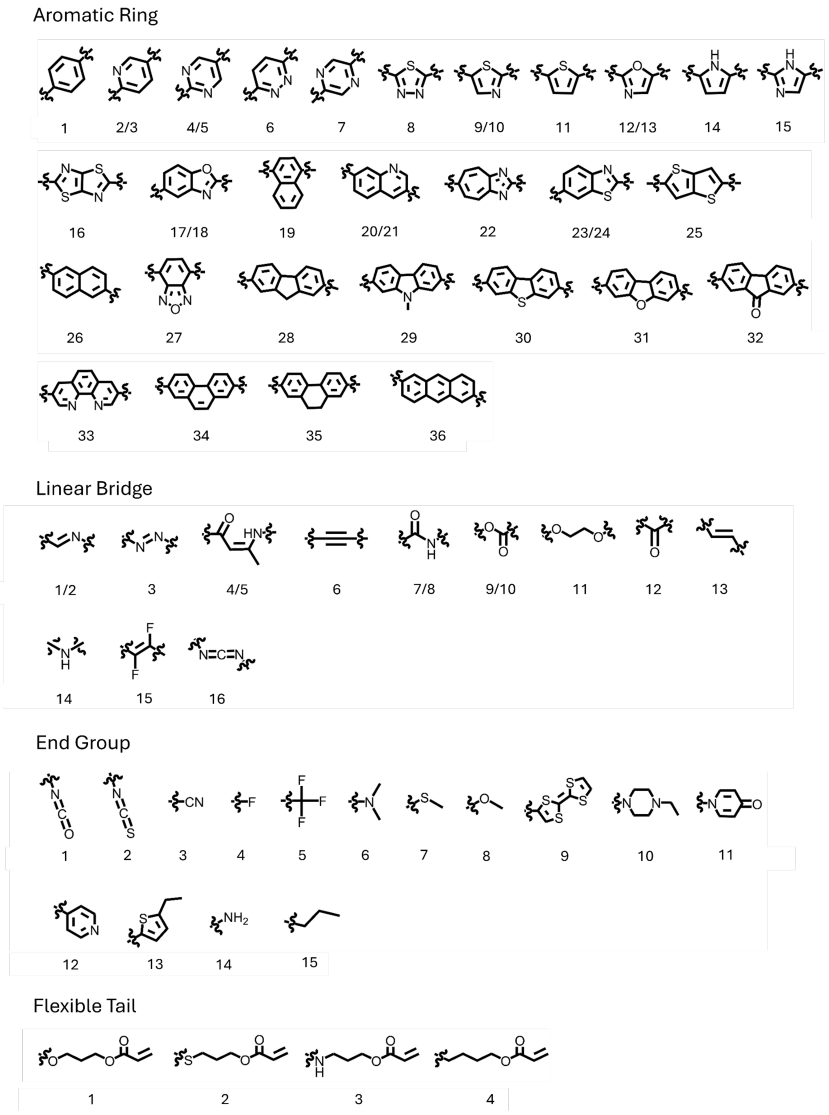

Figure S12: Building blocks list of the four components constituting the reactive mesogen structure: aromatic rings, linear bridges, tails, and end groups. Several of aromatic rings and linear bridges are represented with two indices, meaning that there in an extra choice on the connectivity direction.

References

1. C. Lu, C. Wu, D. Ghoreishi, W. Chen, L. Wang, W. Damm, G. A. Ross, M. K. Dahlgren, E. Russell, C. D. Von Bargen *et al.*, *Journal of chemical theory and computation*, 2021, **17**, 4291–4300.

2. L. Schrödinger, *Schrödinger Release 2024-3: Materials Science Suite*, 2024.

3. L. Schrödinger, *Schrödinger Release 2024-3: Force Fields*, 2024.

4. S. Nosé, *The Journal of chemical physics*, 1984, **81**, 511–519.

5. W. G. Hoover, *Physical review A*, 1985, **31**, 1695.

6. G. J. Martyna, D. J. Tobias and M. L. Klein, *The Journal of chemical physics*, 1994, **101**, 4177–4189.